




Dynamic mechanical characteristics of aged silicone rubber blend

Eman A. Mwafy¹ · M. S. Gaafar² 

Received: 26 May 2022 / Revised: 16 September 2022 / Accepted: 22 September 2022 /
Published online: 2 October 2022
© The Author(s) 2022

Abstract

The effect of aging on the mechanical properties of silicone rubber (SR) was investigated by means of ultrasonic, dynamic mechanical analysis, and FTIR techniques. Both longitudinal and shear (Ultrasonic wave velocities) were measured at room temperature and at frequencies of 2 MHz. Density, molar volume, ultrasonic wave velocities, tensile strength, mechanical properties, and FT–IR showed the improvement of the silicone rubber network with aging time from 0 to 70 days, while loosening of the network structure was observed at 14 days and 50 days aging. These behaviours were explained in terms of the change in cross-link density and average stretching force constant of bonds with aging. Thermogravimetric analysis and differential scanning calorimetric techniques showed quite low thermal stability and temperature performance for aged SR at 14 and 50 days than virgin SR which was confirmed by the cracks and voids appeared under scanning electron microscope.

Keywords Silicone rubber · Ultrasonic wave velocity · Mechanical properties

Introduction

Silicone rubber (SR) is one of the most common semi-organic synthetic polymers known as silicones that look and feel like organic rubber and has completely different types of structures than other elastomers [1–9]. The backbone of the elastomer is not a chain of carbon atoms but an arrangement of silicone and oxygen atoms. This structure gives a very flexible chain with weak inter-chain forces. This accounts for the remarkable small change in dynamic characteristics over a wide range of

✉ Eman A. Mwafy
emanmwafynrc@gmail.com

¹ Physical Chemistry Department, Inorganic Chemical Industries and Mineral Resources Division, National Research Centre, 33 El Bohouth st. (former El Tahrir st.), P.O. 12622, Dokki, Giza, Egypt

² National Institute of Standards, P.O Box: 136, El-Haram, Giza 12211, Giza, Egypt

temperature. They show no molecular orientation or crystallization on stretching and are strengthened by reinforcing materials. However, SR is usually preferable in high-temperature applications, due to the high thermal stability of poly (dimethylsiloxane) (PDMS) and their resistance toward the oxidative degradation. Moreover, silicone elastomers have excellent chemical resistance, thermal and environmental stability over wide temperature range with a good degradation resistance against UV exposure and extreme temperatures [10, 11].

A.N. Chaudhry et al. studied the effect of aging on compression set behavior of a room temperature vulcanized PDMS foam and some initial studies of the oxidation at high temperatures. They reported that chemi-luminescence is the most sensitive method to monitor thermo-oxidative degradation which also shows that PDMS is extremely stable compared to hydrocarbon polymers [12].

Skinner and Patel reported that SR aged in a closed system was softened with time, while air aged samples did not show the same behavior. They proposed that the resulting compression set is due to hydrolysis of PDMS. However, polysiloxanes are stable materials with good resistant to general oxidative and thermal aging environments. Particularly, SR retains their mechanical properties and elasticity over wide temperature ranges from -50 to $+75$ °C. This stability candidates them for a special use in commercial and military aircraft in gaskets and sealing rings for sealing strips, ducting, vibration dampers, jet engines and insulation equipment [13].

Silicone rubber (SiR), a crucial inorganic polymer for electrical insulation, underwent several aging treatments by Takuya Kaneko et al. [14]. Following that, the SiR sheets were investigated using nuclear magnetic resonance, indenter modulus, terahertz (THz) absorption spectroscopy, and IR absorption spectroscopy. As a consequence, it has become evident that three different degradation pathways for SiR manifest themselves depending on the state of aging. Cross-linked structures mostly occur when SiR is aged thermally. On the other hand, if SiR is gamma irradiated at a normal temperature, the oxidation of cyclic siloxane at the surface is evident.

Based on the terahertz frequency band vibration properties of silicone rubber materials, a unique high accuracy non-destructive characterization approach was utilized by Li Cheng et al. [15] for which aging of organic materials has been developed. The origins of vibration peaks in the THz band absorption spectra of aged silicone rubber are examined via acceleration test, microscopic characterization, and molecular modeling in order to assess and validate the methodology suggested in this work. Finally, a quantitative calculation technique and the typical peak frequency of old silicone rubber are discovered. In comparison with previous aging tests, this technique has the benefit of not causing sample damage and eliminates the drawbacks of the current THz assay, which necessitates testing in a nitrogen environment.

To our knowledge, this is first time to characterize the mechanical properties of silicon rubber using different parameters of ultrasonic techniques. In this paper, the longitudinal and shear ultrasonic wave velocities were measured, and the elastic properties of the silicone rubber were then determined by the tests of static tensile, mechanical dynamic and the ultrasonic. During the aging time from 0 to 70 days, the elastic properties were also determined. Additionally, this paper attempts to correlate between the change in density, molar volume, ultrasonic wave velocities and

elastic properties to the anticipated structural changes in the silicone rubber network using FTIR spectroscopy.

Materials and methods

The silicone rubber used in this study was supplied by Pharaoh Co., Egypt. The rubber was mixed with 5 wt% ZnO, 1 wt% stearic acid, 20 wt% silica and 0.8 wt% dicumyl peroxide. Mixing was accomplished on a laboratory two-roll mill; 170 mm diameter and 300 mm working distance at a friction speed ratio of 1:1.4. Nextly, the curing characteristics of the rubber mixes were determined at 150 °C according to the technical procedures of ASTM D 2084–07. Test specimens were taken and the rest of the batch passed through the mill into sheets of 6 mm thick and removed from and set for one day at 25 °C at relative humidity of 45% to complete curing process. The curing was carried out using the oscillating disk rheometer, MRD 2000, Alpha Technology, UK. All samples were cut with the slandered specimens for mechanical measurements.

FTIR spectra of SR were recorded at wave number range between 200 and 4000 cm^{-1} with a resolution of 2 cm^{-1} using JASCO, FT/IR–430 spectrometer (Japan). The infrared spectra were corrected for the dark current noises and normalized to eliminate the concentration effect of the powder sample in the KBr disk. The thermal degradation and differential analysis were studied using the PerkinElmer thermogravimetric analyzer. The morphology was analyzed by scanning electron microscopy (SEM, Quanta FEG 250, FEI, Republic of Czech). For the measurement of mechanical properties as tensile dumbbell specimens were cut from the 2 mm thick sheets and tested by tensile testing machine (Model Z010, Zwick, Germany) at a temperature of 23 ± 2 °C and a crosshead speed of 500 mm/min according to **ASTM D412**. The samples were aged in an air circulating oven for different time durations 0, 2, 4, 7, 14, 20, 30, 40, 50, 60 and 70 days, while the dynamic mechanical analysis (DMA) was carried out on Q800 (TA instruments) by the stress-/strain-controlled force mode and the tension clamp. The sample dimensions were set to 20 mm long, 6 mm wide and 2 mm thick. The hardness of the silicon rubber samples was measured using shore A hardness tester (Zwick 3150, Germany). The density (ρ) of all silicone rubber samples was calculated employing Archimedes principle using toluene as immersion liquid and applying the relation [16, 17];

$$\rho = \rho_b \left(\frac{W_a}{W_a - W_b} \right) \quad (1)$$

where ρ_b is the density of the buoyant, W_a and W_b are the sample weights in air and the buoyant, respectively. The experiment was repeated three times with an error in density measurement which in all silicone rubber samples is $\pm 1 \text{ kg/m}^3$. The molar volume (V_m) has been also calculated as (M/ρ) with accuracy $\pm 0.04 \text{ (m}^3/\text{mol)}$, where M is the molar weight of the polysiloxane rubber. The ultrasonic wave velocities measurements were carried out applying pulse – echo technique by measuring the elapsed time between the initiation and the receipt of the pulse appearing on

the screen of a flaw detector (USM3-Kraüt Kramer) using standard electronic circuit (Hewlett Packard 54615 B). Therefore, the velocity was calculated by dividing the round-trip distance by the elapsed time according to the relation [18];

$$U = \frac{2x}{\Delta t} \quad (2)$$

where x is the sample thickness and Δt is the time interval. All velocity measurements in this study were carried out at 2 MHz frequency and at room temperature 298 K. The estimated error in velocity measurements was ± 1 m/s for longitudinal wave velocity and ± 2 m/s for shear wave velocity. The attenuation coefficient (α) is then calculated from the following equation [19]:

$$\alpha = \frac{20 \log (l_1/l_2)}{2x} \quad (3)$$

where l_1 and l_2 are heights of two successive echoes appeared on the cathode ray oscilloscope. The estimated accuracy of ultrasonic attenuation is about ± 0.3 dB/cm. Also, Elastic moduli (shear (G) and Young's (E)), micro-hardness (H), longitudinal modulus (L), as well as Poisson's ratio (σ) of polysiloxane rubber with aging time from 0 to 70 days have been determined from the measured ultrasonic velocities and density using the relations [20];

$$\begin{aligned} L &= \rho U_l^2 \\ G &= \rho U_s^2 \\ E &= (1 + \sigma) 2G \\ \sigma &= \left(\frac{(L - 2G)}{2(L - G)} \right) \\ H &= \frac{(1 - 2\sigma)E}{6(1 + \sigma)} \end{aligned} \quad (4)$$

Results and discussion

The density and molar volume of solid materials depend on many factors such as coordination number structure, cross-link density, and dimensionality of interstitial spaces [21]. Experimental values of density (ρ) and molar volume (V_m) with aging time are shown in Fig. 1. The density values were found to increase from 1295 to 1315 (kg/m^3) with aging time from 0 to 70 days. Two distinct minima were observed at 14 and 50 days. Otherwise, the values of molar volume of SR were decreased from 57.92 to 57.03 (m^3/mol) with two maxima at 14 and 50 days. As can be seen from Fig. 1, these behaviors are due to the improvement of the dimensionality of polysiloxane rubber structure with aging time from 0 to 50 days. However, both the two minima and maxima in the behaviors of density and molar volume, respectively, at 14 and 50 days, can be returned to the increase in voids in the polymer network

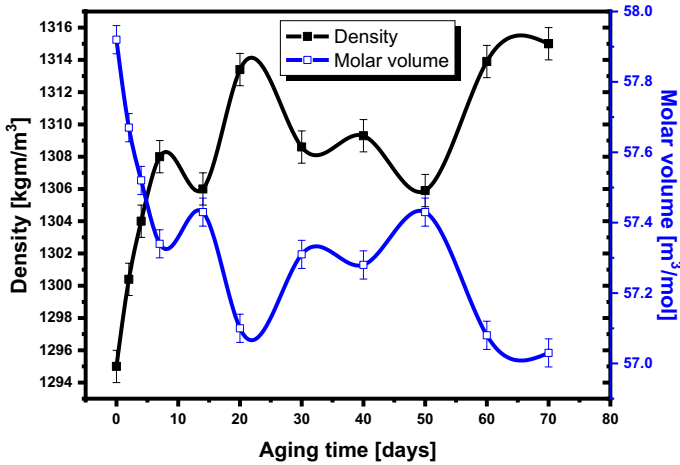


Fig. 1 Dependence of density and molar volume of silicone rubber with aging time

structure and hence the decrease in the cross-link density (as seen in Table 1) which means degradation of the polymer at the aging times of 14 and 50 days. The mechanical properties of SR here were evaluated by different techniques. Among these techniques are static tensile tests, dynamic mechanical tests and by the ultrasonic measurements.

Figure 2a shows the relationship between the tensile strength obtained by static tests and the different aging times. It is clear from the figure that there is a sharp decrease in tensile strength values at 14 days aging and on further increase in the aging time up to 20 days, there is an increase in the tensile strength and remains nearly constant up to 70 days aging except at 50 days aging there is again a small decrease in the tensile strength. The sudden decrease in tensile strength happened at

Table 1 Representation of micro-hardness (H_{ij}) obtained ultrasonically, hardness shore A (H_A), and cross-link density (N_c)

(N_c)	(H_A) Shore A	(H_{ij}) (GPa)	Aging time [days]
0.501 ± 0.012	60.3 ± 0.8	0.0361 ± 0.0002	0
0.501 ± 0.018	80.6 ± 0.8	0.0367 ± 0.0003	2
0.498 ± 0.012	81.4 ± 0.8	0.0368 ± 0.0003	4
0.520 ± 0.012	78.4 ± 0.8	0.0385 ± 0.0002	7
0.426 ± 0.010	78.2 ± 0.8	0.0313 ± 0.0003	14
0.514 ± 0.012	81.9 ± 0.8	0.0383 ± 0.0002	20
0.511 ± 0.012	80.5 ± 0.8	0.0386 ± 0.0002	30
0.514 ± 0.012	81.2 ± 0.8	0.0388 ± 0.0002	40
0.459 ± 0.016	79.9 ± 0.8	0.0344 ± 0.0003	50
0.578 ± 0.014	87.7 ± 0.8	0.0435 ± 0.0002	60
0.660 ± 0.017	89.2 ± 0.8	0.0491 ± 0.0002	70

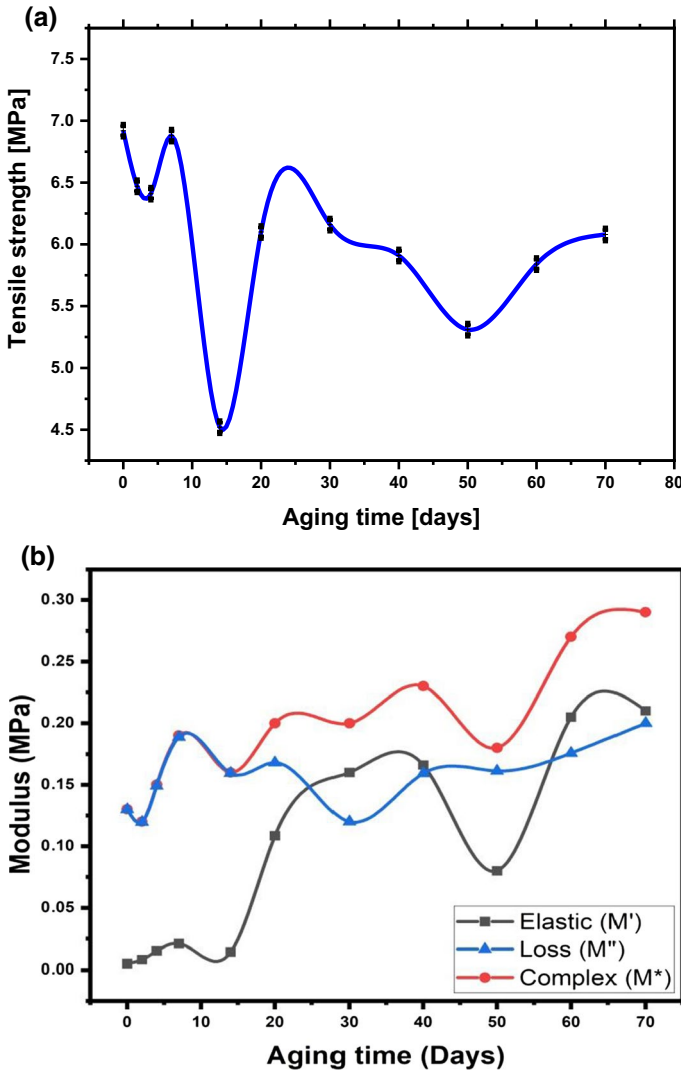


Fig. 2 Variation in **a** Tensile strength and **b** elastic modulus (M), Loss modulus (M''), and complex modulus (M^*) of silicone rubber with aging time

14 days and 50 days aging, may be due to some damage occurs in the delayed cross-links formed during thermal aging [22, 23]. The relationship of the calculated elastic modulus (M) from the static tensile measurements, loss modulus (M''), and complex modulus (M^*) of silicone rubber with aging time and aging time is shown in Fig. 2b. It can be noticed that there is a similar trend as shown in Fig. 2a, b, i.e., there is a noticeable decrease in the elastic modulus values at 14 days and 50 days aging.

The modulus of a material is defined as the overall resistance of the substance to deformation. Polymers display two sorts of behaviors during their transition from

the glassy state to the rubbery state and then to the viscous state, whereas one type of behavior predominating during each transition state. The viscous reaction, or loss as a result of applied stress over strain, is denoted by loss modulus (M''), which denotes the material’s ability to store and dissipate energy as heat, respectively. The phrase complex modulus M^* refers to the sum of real and imaginary modulus’s components.

The variation in the storage modulus (M') and the loss modulus (M'') was studied in this investigation as a function of aging time (cross-linking time), while frequency remains constant. Trends in the variations in storage and loss moduli at various aging times are somewhat boosted. The results showed that under fixed shear oscillation frequency and shear stress, the storage modulus M' steadily increased, corresponding to the creation of internal cross-linking. In actuality, the apparent loss of aged silicon rubber increases with aging time due to a rise in cross-linking generated during aging under temperature, which leads to the strengthening of these cross-links. As a result, molecular mobility along the rubber macromolecular chain is significantly hampered, causing modulus to rise. On the other hand, it was noticed that the value of M' and M'' has dropped in a significant days and in sequence in M^* value, which could be attributed to the formation of some cracks and voids as confirmed by the micrographs taken throughout SEM images, causing an increase in free volume, which causes the sample’s glass transition temperature to move toward the low temperature of lower stiffness and strength. Since the loss factor is the ratio of the energy dissipation modulus to the storage modulus, it can be noticed that the sample’s loss modulus decreases faster during the aging process, implying that the rate at which molecules cross-link during post-solidification and oxidation is faster than the unwinding speed of molecular chains. Furthermore, the drop in storage modulus of the rubber may be linked to that rubber being entangled at this stage of aging, resulting in a decrease in the strength of the rubber and a decrease in the modulus. [24], whereas complex modulus is the sum of real and imaginary modulus’s components so that it showed the same behavior of both M' and M'' for all aging days.

The term ultrasonic attenuation is used throughout to mean the quantified energy losses after the propagation of ultrasonic waves through the material. Rajendran et al. expressed the attenuation coefficient in a solid material by [25]:

$$\alpha = a_1\alpha_a + a_2\alpha_b + \alpha_c + \alpha_d + \alpha_e \tag{5}$$

where a_1 and a_2 are constants, α_a is the true ultrasonic absorption, α_b is the scatter loss, α_c is the coupling loss, α_d is the diffraction loss and α_e is the losses due to the non-parallelism and surface toughness. Due to the amorphous character of the investigated sample, parallelisms of opposite faces and minute thickness of the bonding material between the sample and the transducer and the coefficients α_b , α_d and α_e are negligible. Consequently, Eq. (5) can be rewritten for the examined samples as [26];

$$\alpha = a_1\alpha_a + \alpha_c \tag{6}$$

Figure 3 illustrates how the ultrasonic attenuation changes with the structure of polysiloxane rubber at different frequencies (1, 2 and 4 MHz) with prolonged aging

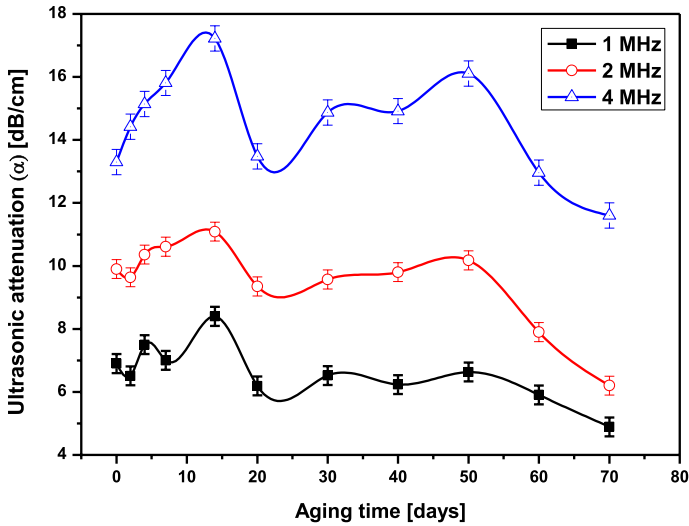


Fig. 3 Variation in ultrasonic attenuation (α) of silicone rubber with aging time

time from 0 to 70 days. The presence of two maxima at both 14 and 50 days in the attenuation behavior reveals the weakening nature of the structure and supports the results obtained from the density and molar volume (V_m) [27].

The relationship between ultrasonic wave velocities (longitudinal and shear) with aging time for the investigated samples is shown in Fig. 4. Both longitudinal (U_l), and shear (U_s) wave velocities were found to increase from 999 and 500 (m/s), respectively, to 1038 and 544 (m/s) with the increase in aging time from 0 to 70 days. However, the behavior of both U_l and U_s ultrasonic wave velocities showed two minima at 14 days and 50 days [28].

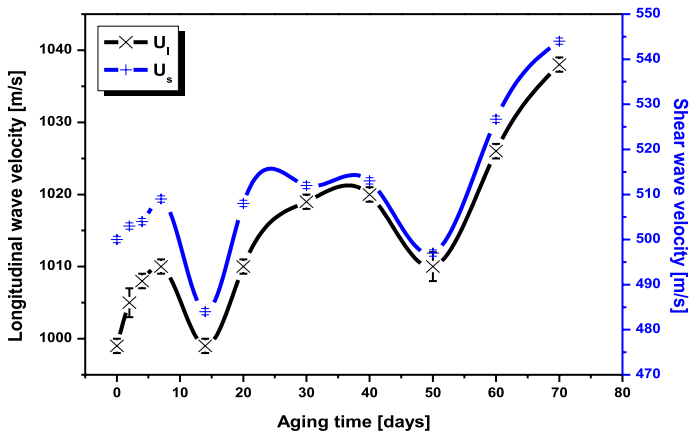


Fig. 4 Relation between ultrasonic wave velocities (U_l and U_s) of silicone rubber with aging time

Generally, the increase in ultrasonic wave velocity is attributed to the decrease in inter-atomic spacing of SR (i.e., the decrease in molar volume). This means that the structure of the silicone rubber has been improved with the increase in the aging time from 0 to 70 days. Moreover, the presence of the two minima in both ultrasonic wave velocities indicates the decrease in cross-link density at 14 days and 50 days.

The observed increase in both Young’s (E) and shear (G) elastic properties of the silicone rubber with aging from 0 to 70 days as shown in Fig. 5 can be interpreted through two approaches. The first one is related to the increase in cross-linking density as seen from Table 1, besides the increase in stretching force constant (F) which will be discussed in the FTIR section. The second approach can be explained by considering the decrease in volume that would lead to an increase in elastic modulus with the increase in the aging time from 0 to 70 days due the decrease in the voids in the polymer network structure. The presence of two minima elastic moduli at 14 days and 50 days aging time can be accounted for the decrease in cross-link density, which means the degradation of the polymer network structure at these two aging times.

It can be seen from Table 1 that micro-hardness (H_V) determined ultrasonically has the same trend as the elastic modulus with the increase in aging time from 0 to 70 days, and hence, the observed increase in (H_V) is related to the increase in the rigidity of the rubber. The presence of two minima observed at 14 days and 50 days confirms the results of elastic moduli [29].

According to Rao [30], Poisson’s ratio (σ) (which is defined as the ratio of the lateral to longitudinal strain when applied force parallel to the chains, therefore increased cross-links will lead to the decrease in lateral strain and consequently the decrease in Poisson’s ratio, and vice versa) depends on the dimensionality of the structure and cross-link density. The cross-link density (N_c) was calculated according to Higazy and Bridge [31] using the following the equation:

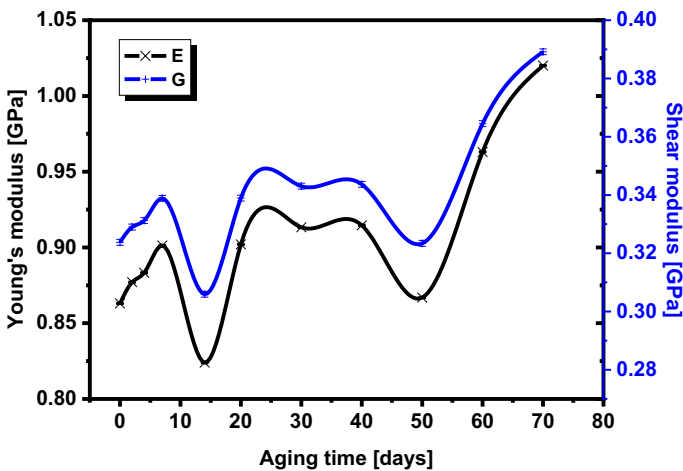


Fig. 5 Variation in Young’s and shear moduli of silicone rubber with aging time

$$\sigma = 0.28(N_c)^{-0.25} \quad (7)$$

Poisson's ratio is inversely proportional to the cross-link density. Therefore, the decrease in Poisson's ratio as shown in Fig. 6 caused the increase in cross-link density with the increase in aging time from 0 to 70 days. Further, the decrease in cross-linking density at 14 days and 50 days aging time confirms the polymer degradation at these two aging times.

The hardness tests measured by "Shore A" hardness tester are shown in Table 1. Results show that there is a sharp increase in the hardness (H_A) values at the beginning of the aging days. This is mainly due to the formation of the cross-links in the polymer followed by a decrease at 14 days due to the degradation of some cross-links formed. With further aging from 20 to 40 days, there is almost no change in the hardness values. This indicates the stability of the cross-links formed, while with prolonged aging up to 50 days, the hardness decreases again due to the deterioration of some of the formed cross-links and increases again with prolonged aging time. These results agree well with the micro-hardness results obtained ultrasonically.

Figure 7 shows FTIR spectrum of SR before and after aging, whereas the main bands associated with the polymer are seen at around 2960 cm^{-1} which assigned to the symmetric C–H stretching of CH_3 groups [32–36]; 1258 cm^{-1} assigned to the symmetric bending vibration of Si–Me bonds with methyl groups; 1008 cm^{-1} assigned to asymmetric stretching of Si–O–Si bonds and 788 cm^{-1} assigned to the vibration of Si–Me bonds with methyl groups [37]. Such figure describes the following;

According to a comparison of the Si–O–Si absorption peak heights (1006 cm^{-1}) for each sample, samples with longer hot air aging times had a somewhat higher Si–O–Si absorption peak (Fig. 8). Due to the silicone rubber's susceptibility to heat during usage, this material's weak Si–O–Si main chain may be broken, causing

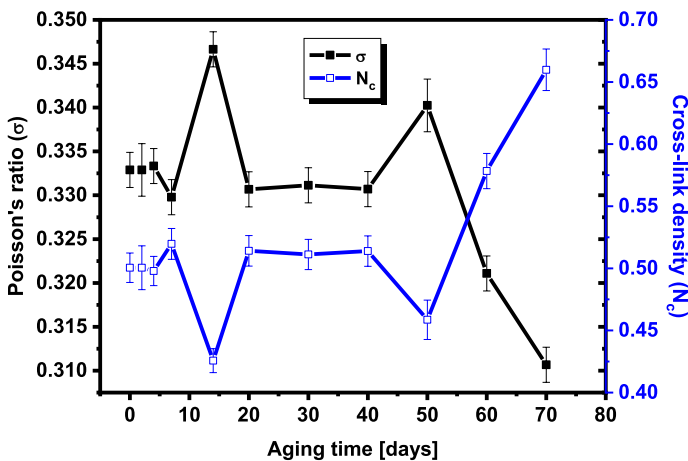


Fig. 6 Dependence of Poisson's ratio and cross-link density of silicone rubber with aging time

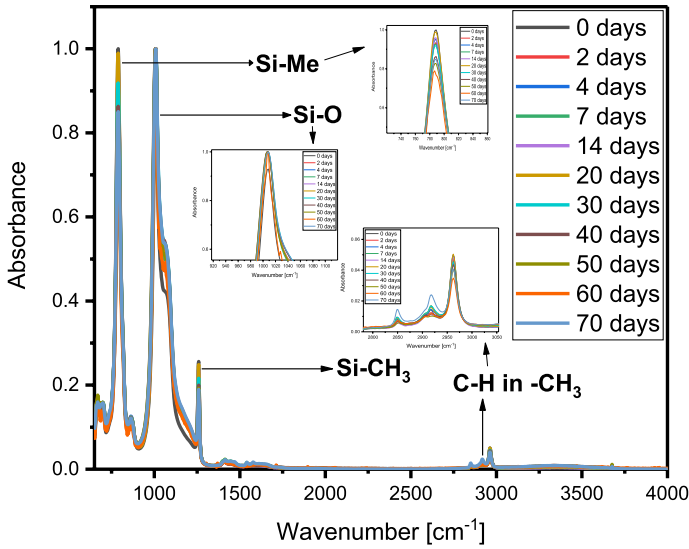


Fig. 7 Normalized FTIR spectrum of the silicone rubber before aging

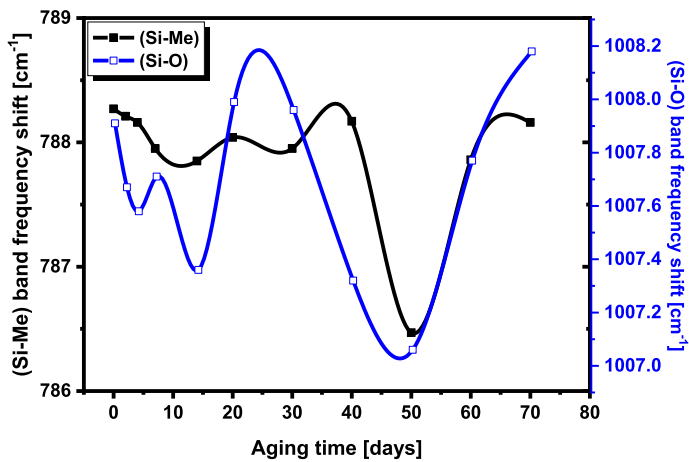


Fig. 8 Band frequency shift of both (Si–Me) and (Si–O) bands at 788 and 1008 cm^{-1} , respectively, with aging time from FTIR results

oxidative cross-linking [38], which increases the amount of Si–O–Si present and increases the height and area of the Si–O–Si absorption peak.

After hot air aging, the silicone rubber’s Si–CH₃ absorption peak intensity was somewhat lower. Due to the fact that the binding energy of Si–C in silicone rubber is lower (301 kJ/mol) than that of Si–O (447 kJ/mol) and C–H (414 kJ/mol). Si–CH₃ is hence more readily obliterated during hot air aging.

Figure 8 shows variation in the frequency shift of all aged samples from 0 to 70 days of the bands at 788 and 1008 cm^{-1} with aging time from 0 to 70 days. It

is clearly seen from this figure that there are two minima of the two band frequencies at 14 days and 50 days. According to Takuya Kaneko et al. [14], SiR hardens substantially when the ratio of Si–O–Si to Si–CH₃ approaches 1.3, suggesting the production of cross-linked structures. The relationship between the bands' ratio [1008 cm⁻¹/788 cm⁻¹] and aging durations between 0 and 70 days is shown in Fig. 9. This graph makes it evident that silicone rubber material is impacted by heat during use due to the occurrence of two reductions in the ratio at 14 and 50 days, which correspond to drops in cross-links at particular aging durations.

Two silica-based composites with 10% micro+5% nano and 15% microsilica were created by Abraiz Khattak et al. in room temperature vulcanized silicone rubber (RTV-iR) [39]. In a specially constructed laboratory, prepared samples were exposed to accelerated conditions such UV radiation, acid rain, heat, and fog for 9,000 h. In a silicone rubber microcomposite containing 15% microsilica, FTIR measurement revealed a progressive rise in the absorption peak at 2963–2960 cm⁻¹, indicating the transfer of a hydrophobic methyl group from the material's bulk to the surface. Similar to the previous example, albeit Si–CH₃ symmetric bending initially decreased more quickly, it recovered and only exhibited a 5% decline after 9000 h. As a result, in the current work, the increase in absorption band intensity around 2962 cm⁻¹ at times after 20 and 50 days, respectively, (see Fig. 10) can be explained as being caused by the transfer of hydrophobic methyl group from the material bulk to the surface, indicating the smoothness, as will be seen in the scanning electron microscopy part. In addition, after 14 and 50 days, respectively, the band about 2962 cm⁻¹ diminished, suggesting the transfer of methyl group from the surface to the bulk material, supporting our findings of increasing surface roughness as shown in the scanning electron microscopy section.

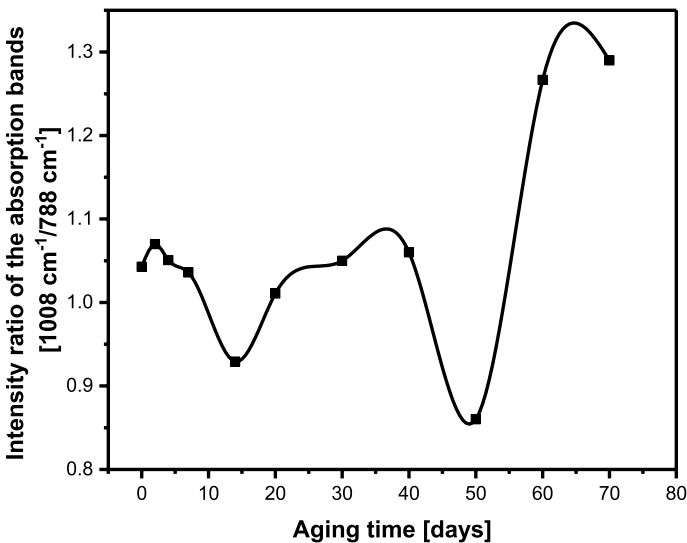


Fig. 9 The relation between the ratio of the bands [1008 cm⁻¹/788 cm⁻¹] as a function of aging times

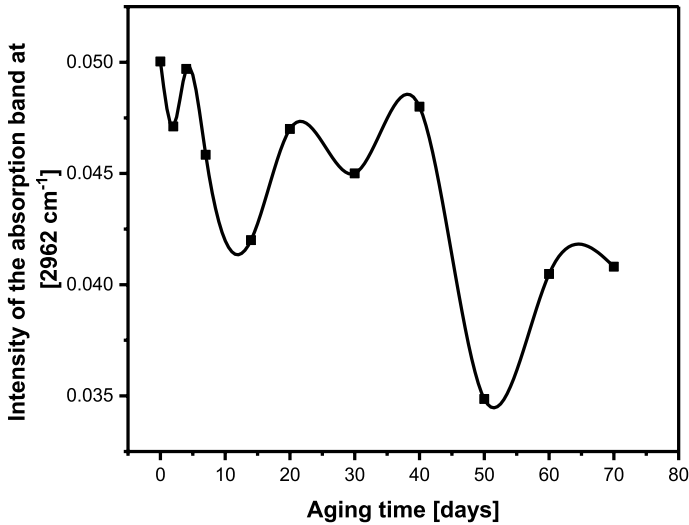


Fig. 10 The relation between the absorption band at 2962 cm⁻¹ as a function of aging times

Thermal properties are essential features of SR that explain the thermal decomposition process. The thermal stability of the silicone rubber was examined through thermogravimetric analysis (TGA) and differential scanning calorimetry (DSC). TGA was performed with a heating rate of 10 °C min⁻¹ under a nitrogen atmosphere. TGA weight loss curve and degradation rate of the synthesized SR demonstrated that the synthesized silicone rubber was started to decompose around 300 °C, while the intensive mass loose was started at 480 °C and ended at around 600 °C with a total mass loose amount of virgin SR is 55% of starting mass of the virgin SR with a moderate stability [32, 40, 41].

After the thermal aging, as shown in Fig. 11a, it was noted that the weight loss rate was increased with the increase in the aging time for 14 and 50 days. It was

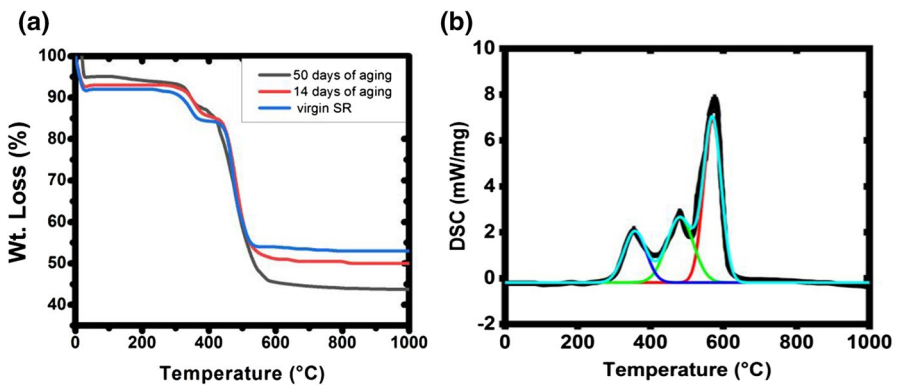


Fig. 11 a TGA of silicon rubber and b DSC of virgin silicon rubber

expected that the methyl group on the side chain was splitted by heating around 300 °C and in the initial stage of weight loss while the another methylene-bridge Si-Me structure was decomposed in the range of 450–500 °C and disappeared in the range of 500–650 °C and the silicon bridge was usually obvious at the higher temperatures level so it is remained because the materials that were hard to decompose were only remained.

In TGA Analysis, C-H methyl group on the side chain plays a main role where the more the methyl groups, (confirmed by FTIR spectrum), the easier the methylene-bridge was to generate. However, after aging, there were more methylene-bridge disappearing at 500–650 °C, but there is more Si bridge were generated in the aging process and they could not easily be decomposed at this temperature range so the weight loss rate was decreased at 500–650 °C. As a result of the increase in the methyl groups amount and the silicon bridge structures after aging process, the thermal stability of SR material was enhanced and the weight loss onset was shifted to the high-temperature region, and the residual mass of silicon rubber decreased with increase in aging time for 14 days and 50 days [42].

The thermogram DSC of silicon rubber as shown in Fig. 11b was conducted with the same heating rate of 10 °C/min illustrating that the most intensive exothermic effect is observed at 580 °C. It is related to the creation of silica phase under heat-treatment.

SEM micrographs are shown in. Figure 12 for SR specimens before and after 14 and 50 days of aging. However, the degradation on the surface is much more serious than the interior indicating that the initial deterioration process began on the surface of the samples and it showed that the surface of the virgin SR was smooth, on which there were no holes, cracks and obvious particles. Under the time aging condition for 14 days and 50 days, the surface of SR samples became rough and appeared a few holes. These appeared cracks on the surface developed in different orientation which severe the easier degradation of SR specimen. The analysis could be a further confirmation for density, molar volume, ultrasonic attenuation and ultrasonic wave velocity, hardness, cross-link density and mechanical properties confirming the polymer degradation at 14 days and 50 days aging.

Conclusions

The density, molar volume, ultrasonic wave velocities, mechanical properties, and FTIR studies on the network structure of silicone rubber with different aging times from 0 to 70 days have revealed the improved mechanical properties with aging due to the improvement of the dimensionality of polysiloxane rubber structure. Drops in the mechanical properties at 14 days and 50 days were attributed to some degradation that occurs in the cross-links formed during thermal aging. The mechanical characteristics acquired by ultrasonic and DMA methods, which confirmed the increasing surface roughness at such aging durations, were supported by FTIR and SEM data that demonstrated reduced cross-linked structures at 14 and 50 days, respectively.

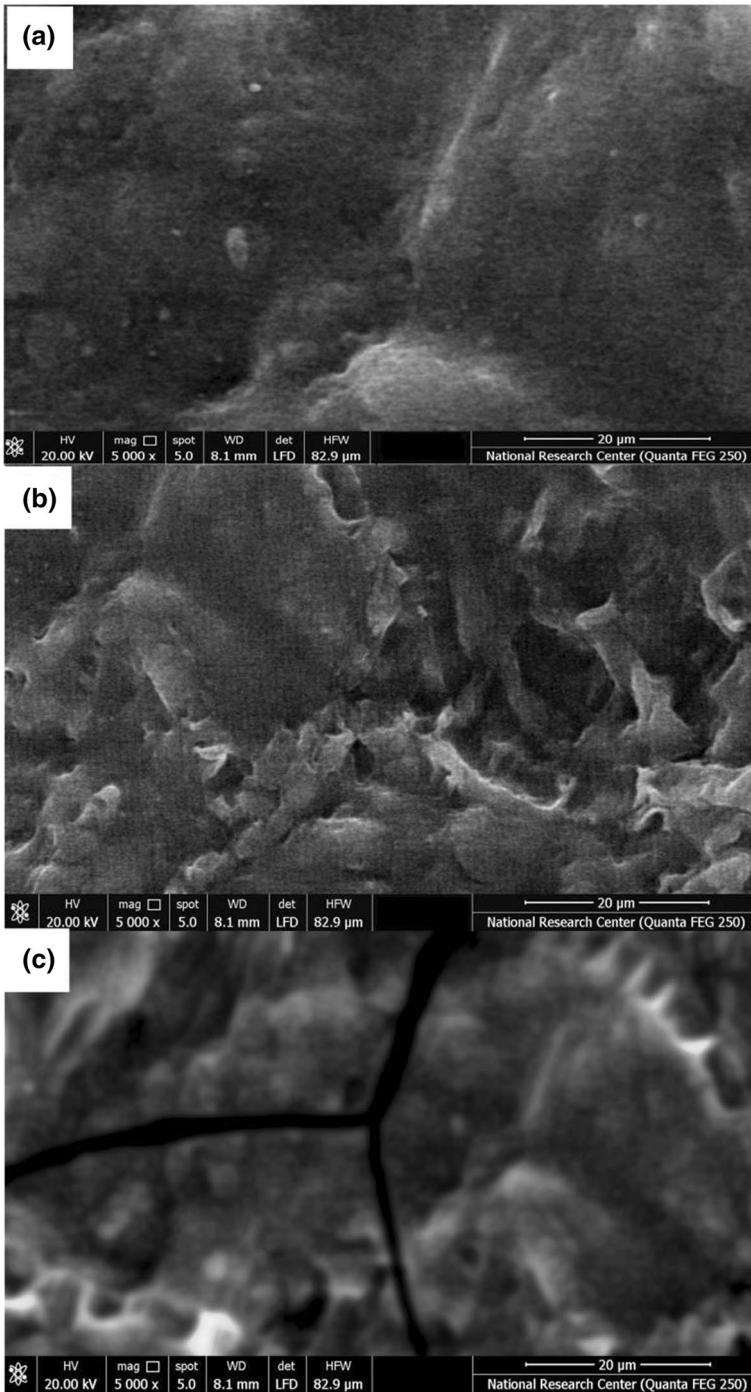


Fig. 12 Scanning electron microscope of silicon rubber **a** virgin SR, **b** aged for 14 days, and **c** aged for 50 days

Acknowledgements The authors wish to express their gratitude to the facilities of National Research Centre and National Institute of Standards in Egypt.

Funding Open access funding provided by The Science, Technology & Innovation Funding Authority (STDF) in cooperation with The Egyptian Knowledge Bank (EKB).

Declarations

Conflict of interest The authors declare that they have no known competing financial interests or personal relationships that could have appeared to influence the work reported in this paper.

Open Access This article is licensed under a Creative Commons Attribution 4.0 International License, which permits use, sharing, adaptation, distribution and reproduction in any medium or format, as long as you give appropriate credit to the original author(s) and the source, provide a link to the Creative Commons licence, and indicate if changes were made. The images or other third party material in this article are included in the article's Creative Commons licence, unless indicated otherwise in a credit line to the material. If material is not included in the article's Creative Commons licence and your intended use is not permitted by statutory regulation or exceeds the permitted use, you will need to obtain permission directly from the copyright holder. To view a copy of this licence, visit <http://creativecommons.org/licenses/by/4.0/>.

References

1. Shit SC, Shah P (2013) A review on silicone rubber. *Natl Acad Sci Lett* 36:355–365
2. Harris AK, Wild P, Stopak D (1980) Silicone rubber substrata: a new wrinkle in the study of cell locomotion. *Science* 208:177–179
3. Mostafa AM, Lotfy VF, Mwafy EA, Basta AH (2020) Influence of coating by Cu and Ag nanoparticles via pulsed laser deposition technique on optical, electrical and mechanical properties of cellulose paper. *J Mol Struct* 1203:127472
4. Mostafa AM, Mwafy EA, Lotfy VF, Basta AH (2019) Optical, electrical and mechanical studies of paper sheets coated by metals (Cu and Ag) via pulsed laser deposition. *J Mol Struct* 1198:126927. <https://doi.org/10.1016/j.molstruc.2019.126927>
5. Mwafy EA, Abd-Elmgeed A, Kandil A, Elsabbagh I, Elfass M, Gaafar M (2015) High UV-shielding performance of zinc oxide/high-density polyethylene nanocomposites. *Spectrosc Lett* 48:646–652
6. Awad A, Abou-Kandil AI, Elsabbagh I, Elfass M, Gaafar M, Mwafy E (2015) Polymer nanocomposites part 1: structural characterization of zinc oxide nanoparticles synthesized via novel calcination method. *J Thermoplast Compos Mater* 28:1343–1358
7. Abou-Kandil AI, Awad A, Mwafy E (2015) Polymer nanocomposites part 2: optimization of zinc oxide/high-density polyethylene nanocomposite for ultraviolet radiation shielding. *J Thermoplast Compos Mater* 28:1583–1598
8. Wang Y, Cai Y, Zhang H, Zhou J, Zhou S, Chen Y, Liang M, Zou HJP (2021) Mechanical and thermal degradation behavior of high-performance PDMS elastomer based on epoxy/silicone hybrid network. *Polymer* 236:124299
9. Hsissou R (2021) Review on epoxy polymers and its composites as a potential anticorrosive coatings for carbon steel in 3.5% NaCl solution: computational approaches. *J Mol Liquids* 336:116307. <https://doi.org/10.1016/j.molliq.2021.116307>
10. Cai D, Neyer A, Kuckuk R, Heise HM (2010) Raman, mid-infrared, near-infrared and ultraviolet–visible spectroscopy of PDMS silicone rubber for characterization of polymer optical waveguide materials. *J Mol Struct* 976:274–281
11. Jin H, Bing W, Jin E, Tian L, Jiang Y (2020) Bioinspired PDMS–phosphor–silicone rubber sandwich-structure coatings for combating biofouling. *Adv Mater Interfaces* 7:1901577
12. Chaudhry AN, Billingham NC (2001) Characterisation and oxidative degradation of a room-temperature vulcanised poly(dimethylsiloxane) rubber. *Polym Degrad Stab* 73:505–510

13. Patel M, Skinner AR (2001) Thermal ageing studies on room-temperature vulcanised polysiloxane rubbers. *Polym Degrad Stab* 73:399–402
14. Kaneko T, Ito S, Minakawa T, Hirai N, Ohki Y (2019) Stability, Degradation mechanisms of silicone rubber under different aging conditions. *Polym Degrad Stab* 168:108936
15. Cheng L, Liu Y, Cheng Z, Chen R, Zhang S, Liao R, Yuan Y (2022) A novel aging characterization method for silicone rubber based on terahertz absorption spectroscopy. *Polym Testing* 115:107723
16. Quan X, Han R, Shao Y, Niu K (2021) Effect of hollow glass beads on density and mechanical properties of silicone rubber composites. *J Appl Polym Sci* 138:49865
17. Dutta P, Borah K (2022) Dielectric Studies of nano-magnesium silicate and linear low-density polyethylene composite as a substrate for high-frequency applications. *J Electron Mater* 51:5368–5375
18. Saito M, Hashimoto T, Taniguchi J (2017) Fabrication of disk droplets and evaluation of their lasing action. *Opt Lett* 42:4119–4122
19. Mousa A, Kusminarto K, Suparta GB (2017) A new simple method to measure the X-ray linear attenuation coefficients of materials using micro-digital radiography machine. *Int J Appl Eng Res* 12:10589–10594
20. Sidkey M, Gaafar MS (2004) Ultrasonic studies on network structure of ternary $\text{TeO}_2\text{--WO}_3\text{--K}_2\text{O}$ glass system. *Physica B* 348:46–55
21. Eid AM, Farag MA, Abd-ullah Abd El-Rahman K, Mohamed M (2016) Ultrasonic study on complex glass system doped with erbium oxide. *J Mater Res* 31(4):495–505
22. Reinhardt HW, Cornelissen HA, Hordijk DA (1986) Tensile tests and failure analysis of concrete. *J Struct Eng* 112:2462–2477
23. Qiu H, Zhu Z, Wang M, Wang F, Luo C, Wan D (2020) Study of the failure properties and tensile strength of rock-mortar interface transition zone using bi-material Brazilian discs. *Constr Build Mater* 236:117551
24. Maghsoudi K, Vazirinasab E, Jafari R, Momen G (2020) Evaluating the effect of processing parameters on the replication quality in the micro compression molding of silicone rubber. *Mater Manuf Process* 35:1567–1575
25. Lou L, He Z, Li Y, Li Y, Zhou Y, Lin C, Yang Z, Fan J, Zhang K, Yang W (2020) Multifunctional silicone rubber/paraffin@ PbWO_4 phase-change composites for thermoregulation and gamma radiation shielding. *Int J Energy Res* 44:7674–7686
26. Cao MS, Wang XX, Zhang M, Cao WQ, Fang XY, Yuan J (2020) Variable-temperature electron transport and dipole polarization turning flexible multifunctional microsensor beyond electrical and optical energy. *Adv Mater* 32:1907156
27. Zheng S, Zhang S, Luo Y, Xu B, Hao W (2020) Evaluation, Nondestructive analysis of debonding in composite/rubber/rubber structure using ultrasonic pulse-echo method. *Nondestr Test Eval* 36:515–527
28. Saddeek YB, Gaafar MS, Abd El-Aal NS, Abd El-Latif L (2009) Structural analysis of some alkali diborate glasses. *Acta Phys Polonica A* 116(2):211–216. <https://doi.org/10.12693/APhysPolA.116.211>
29. Ye N, Zheng J, Ye X, Xue J, Han D, Xu H, Wang Z, Zhang L (2020) Performance enhancement of rubber composites using VOC-Free interfacial silica coupling agent. *Compos B Eng* 202:108301
30. Rao KJ (2002) *Structural chemistry of glasses*. Elsevier, Amsterdam
31. Higazy AA, Bridge B (1985) Elastic constants and structure of the vitreous system $\text{Co}_3\text{O}_4\text{--P}_2\text{O}_5$. *J Non-Crystalline Solids* 72(1):81–108
32. Mwafy EA (2020) Eco-friendly approach for the synthesis of MWCNTs from waste tires via chemical vapor deposition. *Environ Nanotechnol Monitor Manag* 14:100342
33. El-Saied H, Mostafa AM, Hasanin MS, Mwafy EA, Mohammed AA (2020) Synthesis of antimicrobial cellulosic derivative and its catalytic activity. *J King Saud Univ Sci* 32:436–442
34. El-Messery TM, Mwafy EA, Mostafa AM, Fakhr HM, El-Din AM, Amarowicz R, Ozcelik B (2020) Spectroscopic studies of the interaction between Isolated polyphenols from coffee and the milk proteins. *Surf Interfaces* 20:100558. <https://doi.org/10.1016/j.surfin.2020.100558>
35. Mwafy EA, Mostafa AM (2019) Multi walled carbon nanotube decorated cadmium oxide nanoparticles via pulsed laser ablation in liquid media. *Opt Laser Technol* 111:249–254

36. Mwafy EA, Hasanin MS, Mostafa AM (2019) Cadmium oxide/TEMPO-oxidized cellulose nanocomposites produced by pulsed laser ablation in liquid environment: synthesis, characterization, and antimicrobial activity. *Opt Laser Technol* 120:105744
37. Al-Oweini R, El-Rassy H (2009) Synthesis and characterization by FTIR spectroscopy of silica aerogels prepared using several Si (OR)₄ and R'' Si (OR')₃ precursors. *J Mol Struct* 919:140–145
38. Ma B, Gubanski SM, Hillborg H (2011) AC and DC zone-induced ageing of HTV silicone rubber. *IEEE Trans Dielectr Electr Insul* 18:1984–1994
39. Amin M, Khattak A, Ali M (2018) Accelerated aging investigation of silicone rubber/silica composites for coating of high-voltage insulators. *Electr Eng* 100(1):217–230
40. Mwafy EA, Mostafa AM (2020) Efficient removal of Cu (II) by SnO₂/MWCNTs nanocomposite prepared by pulsed laser ablation in liquid media. *Nano-Struct Nano-Obj* 24:100591
41. Darwish WM, Darwish AM, Al-Ashkar EA (2016) Indium (III) phthalocyanine eka-conjugated polymer as high-performance optical limiter upon nanosecond laser irradiation. *High Perform Polym* 28:651–659
42. Zhao J, Zhang J, Wang L, Li J, Feng T, Fan J, Chen L, Gu J (2020) Superior wave-absorbing performances of silicone rubber composites via introducing covalently bonded SnO₂@MWCNT absorbent with encapsulation structure. *Compos Commun* 22:100486

Publisher's Note Springer Nature remains neutral with regard to jurisdictional claims in published maps and institutional affiliations.